Photocatalytic aerobic oxidative carbonylation of methane by iron terpyridine catalysts

Zhiwei Zuo (zuozhw@mail.sioc.ac.cn)
State Key Laboratory of Organometallic Chemistry https://orcid.org/0000-0002-3361-3220
Hui Pan
ShanghaiTech University
Qing An
ShanghaiTech University
Hui Chen
Shanghai Institute of Organic Chemistry
Yuegang Chen
ShanghaiTech University
Alexander van der Made
Shell
Joost Smits
Shell Global Solutions International BV
Sander van Bavel
Shell Golbal Solut, Gas Convers, Amsterdam, Netherlands

Physical Sciences - Article

Keywords: photocatalytic aerobic oxidative carbonylation, methane

Posted Date: December 28th, 2020

DOI: https://doi.org/10.21203/rs.3.rs-124171/v1

Photocatalytic aerobic oxidative carbonylation of methane by iron terpyridine catalysts

Hui Pan,[†‡] Qing An,[†‡] Hui Chen,[‡¶] Yuegang Chen,[†] Alexander van der Made,[§] Joost Smits,[§] Alexander P. van Bavel [§] and Zhiwei Zuo[‡*]

[†]School of Physical Science and Technology, ShanghaiTech University, Shanghai 201210, China

[‡]State Key Laboratory of Organometallic Chemistry, Shanghai Institute of Organic Chemistry, University of Chinese Academy of Sciences, Shanghai 200032, China;

[¶]School of Chemistry and Materials Science, Hangzhou Institute for Advanced Study, University of Chinese Academy of Sciences.

[§]Shell Global Solutions International BV, PO Box 38000, 1030 BN Amsterdam, the Netherlands

Employing methane as a C1 feedstock for commodity chemicals represents a sustainable and empowering opportunity for chemical catalysis. However, practical demands of industrial development have imposed serve challenges to utilize coeffective catalysts and reagents as well as ecologically benign conditions for highly efficient and selective C(sp^3)–H bond functionalizations, constantly driving the development of catalytic strategies[1,2]. The aerobic oxidative carbonylation of methane represents an ideal approach for sustainable acetic acid synthesis, yet poses a longstanding challenge in selectivity for C2:C1 products[3-8]. In recent years, metallaphotocatalysis in which photoredox catalysts operate in synergy with transition metal catalysts to facilitate both 1- and 2-electron reaction steps, has provided intriguing opportunities to achieve selective cross-couplings otherwise unattainable[9-17]. Here, we demonstrate the utilization of an iron terpyridine catalyst to facilitate multiple 1- and 2-electron processes, including photoexcitation, radical generation, oxidative radical capture and carbonylation, in the form of methane aerobic carbonylation to acetic acid. High levels of catalytic efficiency (turnover numbers up to 31480) and selectivity (C2/C1 ratio up to 142:1) have been achieved with a robust iron terpyridine photocatalyst at ambient temperature under LED irradiation. Importantly, this practical catalytic manifold has been adapted to the selective oxidative carbonylation of various feedstock alkanes.

The catalytic carbonylation of methanol by rhodium and iridium complex, a significant milestone in transition metal catalysis, has dominated the industrial production of acetic acid and has been hugely inspiring for the development of novel carbonylation technologies[18-20]. Instead employing methane directly as a C1 feedstock in the catalytic aerobic carbonylation, exclusively converting inexpensive feedstock materials (i.e. CH_4, CO, and O_2), has drawn considerable research attention[3-8]. Key challenges stem from the chemical inertness of CH_4 and high propensity for oxidation of activated C1 components[21,22]; thus, controlling for aerobic oxidative carbonylation with poorly reactive CO over methane oxidation presents a longstanding challenge in C2/C1 selectivity. Elegant examples using $RhCl_3$ or Rh anchored on zeolite materials have demonstrated moderate to good efficiencies under high temperature conditions, however, the C2/C1 selectivities remain unsatisfactory[3,6-8].

Recently, photoredox catalysis has been demonstrated to be a mild and effective platform for the functionalization of methane through catalytic hydrogen atom transfer (HAT) enabled by cerium and decatungstate photocatalysts[23,24]. Such an approach represents a new paradigm in methane C–H functionalization, operating through highly reactive open-shell methyl radical. However, under aerobic conditions required for practical oxidative carbonylation of methane, the nucleophilic methyl radical would be preferentially trapped by molecular oxygen ($k = 4.7 \times 10^9\ M^{-1}s^{-1}$)[25], as opposed to the sluggish and reversible coupling between methyl radical and CO ($k = 2 \times 10^6\ M^{-1}s^{-1}$)[26,27].

Nature provides inspiration for such a concept, as methane monooxygenase utilizes a radical rebound mechanism to capture incipient methyl radical, suppressing uncontrolled aerobic methane oxidation[28,29]. However, synthetic chemists have heretofore been unable to similarly control the reactivity of methyl radical, and as such radical-mediated carbonylation of methane has operated exclusively under deaerated atmosphere, necessitating the use of strong oxidizing agents[30-33], making acetic acid under conditions impractical for large scale applications. Metal-centered oxidative radical capture, particularly synergistically employed with photoexcitation, has recently emerged as a powerful strategy to overcome reactivity and selectivity challenges in the realm of radical-mediated as well as transition metal catalyzed-coupling processes[9-11,14,17,34-37]. We recently questioned whether a single metal center could facilitate both ligand-to-metal charge

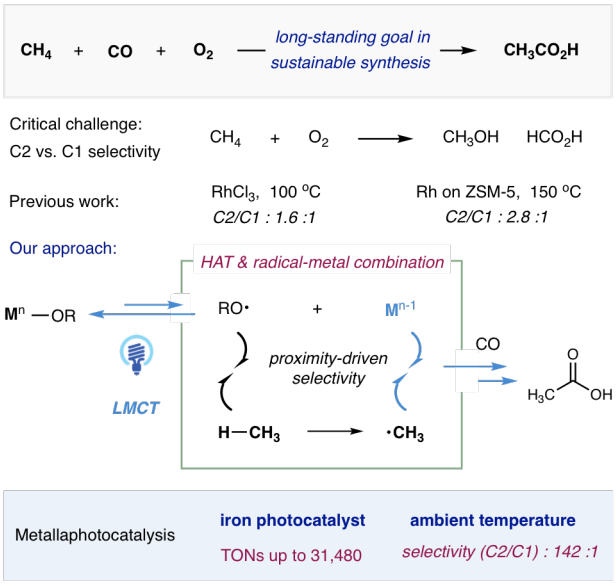

Fig. 1. Photocatalytic aerobic oxidative carbonylation of methane by iron catalyst. A radical-metal combination merged with LMCT-homolysis was proposed to elude the nonselective methane oxidation for highly selective carbonylation.

transfer (LMCT) excitation for the generation of alkoxy radicals and oxidative radical capture by the reduced metal center for the generation of metal-methyl complex. Previously, the low-valent metal generated via LMCT-homolysis has only been invoked for single electron transfer (SET) events merely to achieve catalyst turnover[23]. In this hypothetical reaction manifold, the methyl radical generated through alkoxy radical-mediated HAT would be trapped by the low-valent metal complex in close proximity, in a mechanistically analogous manner to the radical rebound system, to allow diverse utilizations of methyl radicals for practical transformations, specifically methane aerobic carbonylation.

The challenges to fulfill this design lie in the identification of a suitable transition metal species which can undergo LMCT-homolysis in its high oxidation form and in turn combine with nucleophilic alkyl radical in its low valent state. Seminal reports on iron(III) porphyrins drew our attention to iron catalysts[38,39]. It has been established that the *in situ* coordinated iron(III) porphyrin alkoxide complex could undergo photoinduced-ligand homolysis to generate iron(II) and alkoxy radicals under irradiation [40,41], although suppression of reported alcohol oxidation pathways would be required to achieve efficient HAT. Two additional critical precedents establish a rationale for investigating iron complexes. First, iron(II) porphyrin is reported to undergo rapid combination with methyl radical (rate constant, 3.9×10^9 $M^{-1}s^{-1}$) [42]. Second, iron(III) alkyl complexes are well-established to undergo facile CO insertion to generate iron acyl species which could degrade into carboxylates [43,44]. Thus, iron complexes appeared to be an ideal platform for each requisite elementary step for LMCT-mediated aerobic carbonylation of methane.

Considering the enabling capacity of hexafluoroisopropoxy radical in HAT and the deactivation effect of two trifluoromethyl groups [23,45], hexafluoroisopropanol (HFIP) was chosen as the solvent. Gratifyingly, under the irradiation of 400 nm LED (irradiation intensity: 0.37 W cm^{-2}), commercially available iron(III) tetraarylporphyrin **1** indeed led to a small amount of acetic acid at ambient temperature, although with the opposite sense of C2:C1 selectivity desired. Peculiarly, trace amounts of hexafluoroisopropanyl acetate and methyl acetate were also observed. Notably, under the same partial pressure of three gas components, the use of cerium catalyst only resulted in methane oxidation with no C2 products observed. Decatungstate photocatalyst, previously demonstrated capable of generating methyl radical with 365 nm LED excitation [24], was inactive under the current condition.

Intensive efforts of ligand modification eventually led us to identify iron(III) terpyridine complexes, which have not been exploited in LMCT catalysis, as more active and selective photocatalysts for this transformation. Iron(III) terpyridine boosts the production of acetic acid into 757 μmol, generates a total of 803 μmol C2 products with only 74 μmol C1 products formed, demonstrating a high C2/C1 selectivity of 11:1. Importantly, peroxide species, including peracetic acid and methyl peroxide, could not be detected via ^{1}H NMR or chemical reduction methods. The existence of other possible by products, such as ether from the coupling of methyl radical with hexafluoroisopropoxy radical, or chlorinated methanes, were thoroughly checked and precluded by GCMS analysis. No ethane could be detected either at an early stage or after 8 hours of irradiation. However, we did observe the formation of CO_2 (449 μmol), which was confirmed

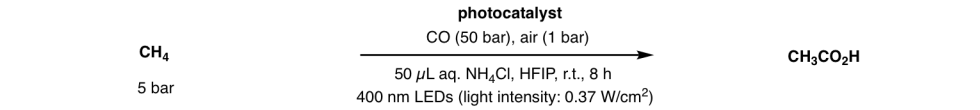

photocatalyst	C2 product		C1 product		Selectivity	TON
	CH_3CO_2H	CH_3CO_2R	CH_3OH	HCO_2H	C2/C1	
$Ce(OTf)_4$ (1 μmol)	0	0	15	18	–	33
TBADT (1 μmol, 365 nm LED)	0	0	0	0	–	–
cat. **1** (0.1 μmol)	11	trace	67	144	0.05:1	2220
cat. **2** (0.1 μmol)	757	46	26	48	11:1	8770
cat. **3** (0.1 μmol)	961	67	22	18	26:1	10680
cat. **4** (0.1 μmol)	746	42	15	36	15:1	8390
cat. **5** (0.1 μmol)	675	46	20	54	9.7:1	7950
cat. **6** (0.1 μmol)	599	38	27	72	6.4:1	7360
cat. **7** (0.1 μmol)	167	8	60	192	0.69:1	4270
cat. **3** (0.05 μmol) 100 bar CO, w/o H_2O, 48 h	1236	327	5	6	142:1	31480
cat. **3** (0.05 μmol) 1 bar CH_4, 100 bar CO, 48 h	714	62	4	12	49:1	15840

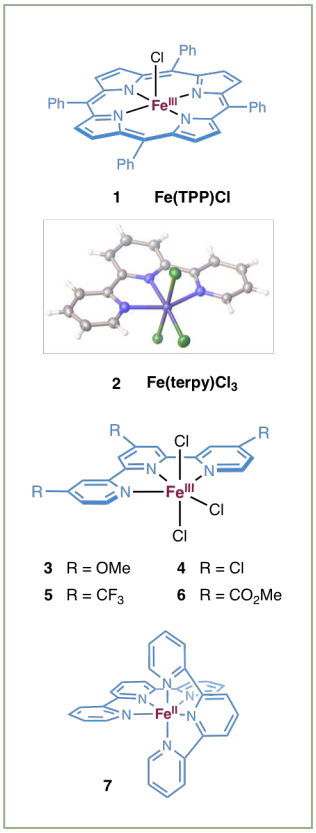

Fig. 2. Selective aerobic oxidative carbonylation of methane. Yields and ratios of all products were determined by GC, ^{1}H NMR analysis with internal standard. See full details in Supporting materials. R = $OCH(CF_3)_2$.

to be derived from aerobic oxidation of CO (vide infra). Considering that photodecarboxylation of acetic acid would be detrimental to the catalytic efficiency, control experiment swapping methane with acetic acid revealed a full recovery of acetic acid after irradiation (see Scheme S1), indicating that the photodecarboxylation is inhibited under the current non-basic setting, probably by virtue of using coordinating solvent.

Remarkably, tuning the electronic property of the terpyridine ligands via the installations of different substitutes has led to intriguing findings towards catalytic efficiency and selectivity. Improved catalytic efficiency was achieved by methoxy substituted iron complex **3**, which promoted the production of C2 products and suppressed methane oxidation, leading to an improved 26:1 selectivity ratio with TONs up to 10680 (turnover frequency, 0.4 s^{-1}). Iron catalysts equipped with electron withdrawing groups such as chloride (**4**), trifluoromethyl (**5**), and carboxylic ester (**6**), nonetheless resulted in somewhat reduced efficiencies for acetic acid and declined selectivity. Bis(terpyridine) iron(II) **7**, a coordinatively saturated and stable iron(II) catalyst, was found to be much less effective in comparison to **2**. The highest production of acetic acid was obtained with 0.05 μmol of **3** under anhydrous conditions, leading to a notable increase in TONs (up to 31480) and almost exclusive formation of C2 products (142:1 C2/C1 selectivity). Without the addition of water, the ratio of HFIP ester to acetic acid slightly increased (1: 3.8). Notably, this highly efficient iron catalyst further allows us to perform the aerobic oxidative carbonylation using 1 bar of methane to acquire 776 μmol of C2 products under the mild conditions. Importantly, a high level of selectivity was maintained and an 8% estimated conversion yield based on methane was obtained[6].

Control experiments revealed an exclusive methane oxidation in the absence of CO, and a photocatalytic CO aerobic oxidation in the absence of methane (see Fig. S1). No reaction took place in the absence of iron catalyst, air or LED light. Furthermore, control experiment utilizing methanol or formic acid to replace methane as the C1 source in this catalytic system only revealed formic acid after irradiation, without any sign of acetic acid, precluding methanol and formic acid as viable intermediates for the carbonylation pathway (see Schemes S2 and S3). Considering that methyl halides have been identified as the active intermediates in transition metal catalyzed carbonylation processes, we then carried out the control experiment with methyl chloride and excluded it as a possible intermediate in this photocatalytic process (see Scheme S4).

To further elucidate the source of each carbon and oxygen atoms of the acetic acid product and gain insights of the mechanism, isotope labelling experiments were then conducted. As demonstrated in Scheme 1A and 1B, when $^{13}CH_4$ was employed, isotope enriched methyl of acetic acid was observed, while isotope enriched carbonyl of acetic acid was observed when ^{13}CO was used. $^{13}CO_2$ was overwhelmingly detected in the ^{13}CO experiment but negligible in the $^{13}CH_4$ experiment, which further revealed that CO_2 is mainly generated from CO aerobic oxidation. ^{18}O isotope tracing experiments revealed the partial incorporation of ^{18}O into acetic acid either when $^{18}O_2$ was employed as the oxidant (Scheme 1C), or excess $H_2{}^{18}O$ was introduced (Scheme 1D). In both experiments, the labelling ratios detected in acetic acid and water are in close range. Taken together, these results are indicative of the provenance of the components of acetic acid as follows: the methyl group derives from methane, the carbonyl carbon derives from CO, and the additional oxygen derives from water, either explicitly added to the reaction or formed in situ by O_2 reduction. Importantly, stoichmetric iron terpyridine complex could act as a viable oxidant to generate acetic acid under anaerobic condition, without the formation of methanol (see Scheme S9). Under this stoichmetric condition, without the interference of water generated from photocatalytic reduction of oxygen, the introduction of ^{18}O water has led to the overwhelmingly labelled acetic acid (98%) (Scheme 1E). These ^{18}O labelling experiments, together with the existence of HFIP ester, all lend support to a nucleophilic attack at the acyl carbonyl (either of acyl-iron complexes or acylium cation) by water or hexafluoroisopropanol as the predominant termination pathway for the formation of C2 products.

The *in situ* formed iron(III) alkoxide complex in HFIP could be isolated and characterized as complex **8** with three alkoxide ligands, which proved equivalently competent in the catalytic aerobic carbonylation of methane. When **8** was irradiated in the presence of neohexene (**9**) and DIAD, product **10** was observed; this product can be rationalized as deriving from HFIP-derived alkoxy radical addition across the olefin and subsequent trapping of the carbon-centered radical by DIAD.

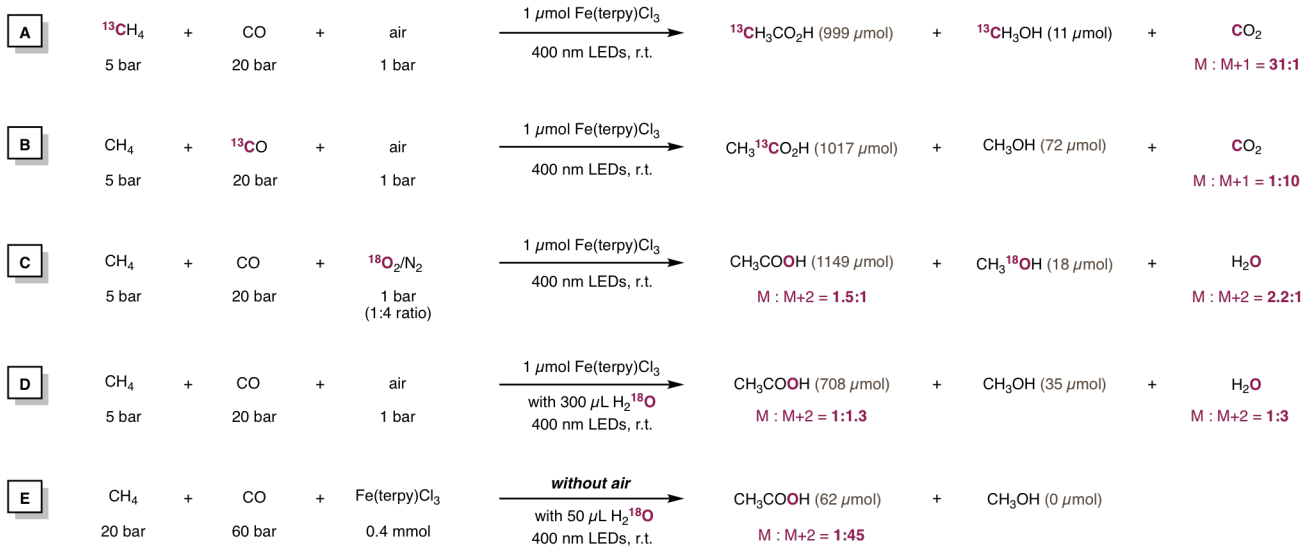

Scheme 1. Isotope labelling experiments.

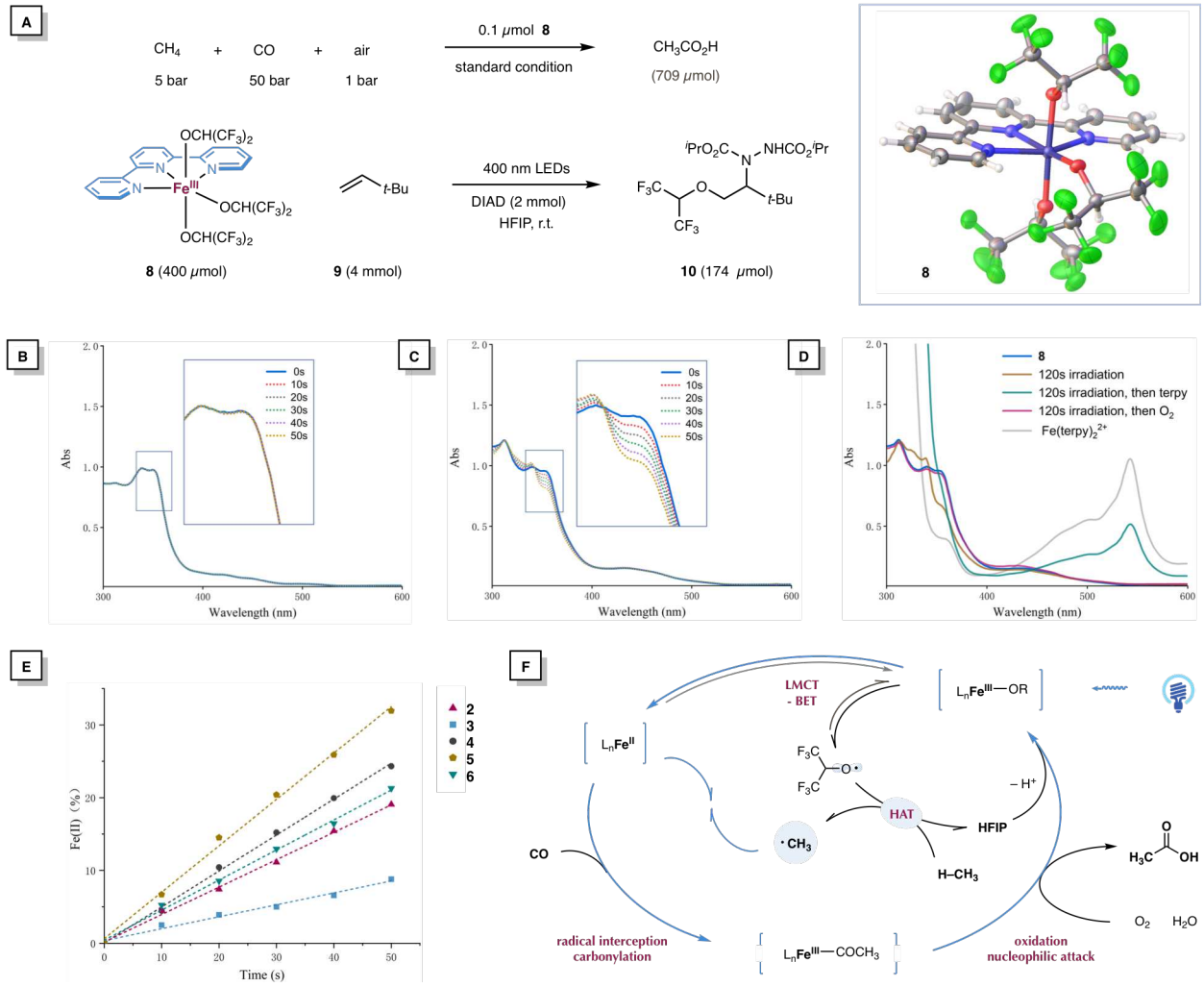

Fig. 4. Mechanistic investigations. (A) Structure elucidation of complex **8** and radical-trapping experiment. (B) Photolysis of complex **8** in HFIP. (C), (D), Photolysis of complex **8** in HFIP, in the presence of neohexene (0.4 M). (E) photolysis rates of various iron alkoxide complexes in the presence of neohexene (0.4 M). (F) A proposed model for the photocatalytic aerobic carbonylation of methane. R = $OCH(CF_3)_2$.

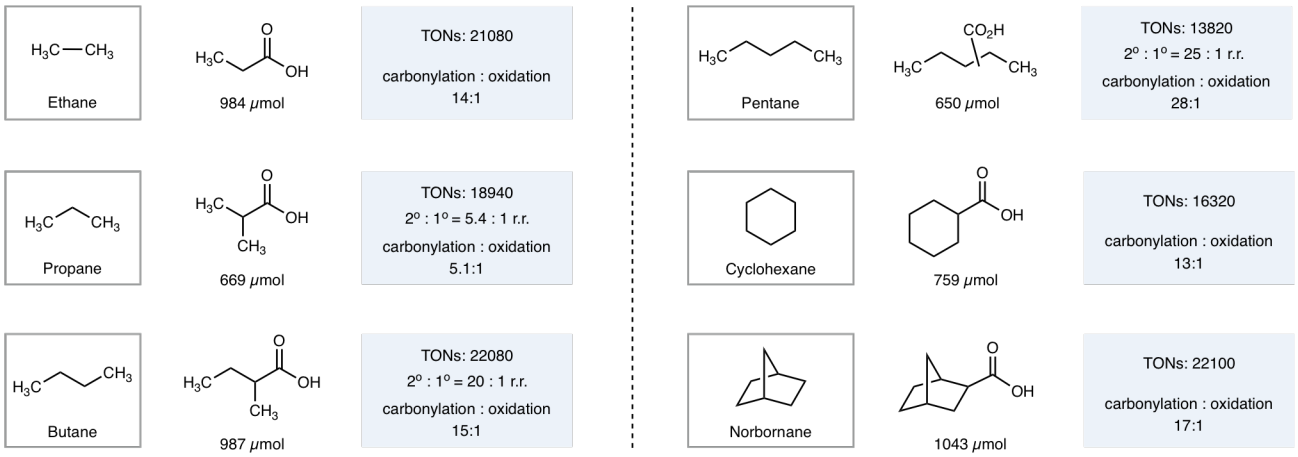

Scheme 2. Photocatalytic aerobic oxidative carbonylation of feedstock alkanes. The reactions were performed using 0.05 umol **3** under ambient temperature. See supporting information for experimental details.

Steady-state photolysis of complex **8**, which exhibits a broad absorption band centered at 355 nm trailing to 500 nm, was carried out. Unexpectedly, the photolysis of the iron(III) complex via constant irradiation with a 375 nm laser (light intensity, 6.3×10^{-8} Einstein s^{-1}) rendered no appreciable spectral changes, indicating no isolated photoactivity of LMCT-homolysis (Fig. 4B). However, simply upon addition of neohexene as a radical trapping species, a fast LMCT-homolysis event was able to be detected. Upon irradiation, photoinduced decay of iron(III) can be assigned by the gradually declining of the broad absorption band centered at 355 nm (Fig. 4C), while the generation of reduced iron(II) species, deriving from Fe(III)-OR bond homolysis, could be detected. In particular, this metal-centered reduction can be more robustly measured when the irradiated solution was treated with an excess amount of terpyridine; then, an absorption band centered at 542 nm, the characteristic absorption band of the bis(terpyridine) iron(II) **7** could be observed (Fig. 4D). If instead, oxygen was introduced into the irradiated solution, the initial iron(III) complex was observed, suggesting oxygen could serve as the oxidant to achieve catalyst turnover. These data present a highly inefficient isolated LMCT-homolysis upon excitation of **8**, which nevertheless is rendered efficient through the inclusion of an O-radical trap, thus delivering isolated Fe(II) species.

With an understanding of the external factors controlling LMCT-homolysis efficiency, we next turned our attention to the metal complex characteristics which influence this key step. Initial rates of photoinduced LMCT-homolysis of iron(III) terpyridine alkoxides in the presence of neohexene were estimated based on the production of Fe(II) (Fig. 4E). Complex derived from **3**, which exhibits a slightly more intensive absorption in visible-light region among these catalysts (see Fig. S7), demonstrates a relatively slow bond-homolysis rate compared to other iron(III)-terpyridine complexes equipped with electron-deficient substitutes. As the rates all showed first-order dependence on olefin concentration (see Fig. S8), it can be concluded that the relative rates of Fe(II) generation of each complex show an inverse dependence on the rate of radical recombination of the fleeting Fe(II) and alkoxy radical species. Thus, it can be concluded that the most electron-rich, reducing Fe(II) species, that derived from **3**, has the fastest rate of radical recombination with hexafluoroisopropoxy radical upon homolysis.

While the observation that the most efficient, selective catalyst for methane aerobic carbonylation has the least efficient bond homolysis step may seem counterintuitive, we posited that this effect is actually crucial to rationalizing the excellent C2:C1 selectivity observed. First, if the rate of Fe(II)-alkoxy radical recombination is very high, a negligible concentration of alkoxy radical will exist in solution, inherently requiring HAT to occur in proximity to the Fe(II) center, setting the stage for radical methyl radical capture at iron. Reinforcing this, the more reducing Fe(II) species derived from **3** would be optimal for oxidative methyl radical capture. Accordingly, taking the kinetics previously measured with structurally similar iron(II) complex into account, the formation of iron-methyl complex would prevail over the coupling of methyl radical with triplet oxygen, thus facilitating acetic acid formation via iron-mediated carbonylation.

A catalytic model was tentatively proposed based on these investigations and insights (Fig. 4F). Under irradiation, the constant photoexcitation of iron(III) alkoxide renders alkoxy radical homolysis and radical recombination on a loop until being interrupted by methane in close proximity. Methyl radical is generated via HAT with hexafluoroisopropoxy radical, and subsequently trapped by the resultant nearby iron(II) complex to produce an iron(III) methyl complex, which would promote CO insertion to generate an acyl iron(III) complex. The degradation of the resultant intermediate, possibly through nucleophilic attack by water or HFIP and an oxidation of the iron center, would generate acetic acid and complete the catalytic cycle.

With a thorough understanding of the reactivity of this catalytic system, we further applied it towards the oxidative carbonylation of various alkane feedstocks (see Scheme 2). Light alkanes including ethane, propane, and butane could be directly transformed into the corresponding one-carbon homologated carboxylic acids with high selectivity for C–H carbonylation vs. C–H oxidation. Importantly, good levels of selectivities of methylene vs. methyl groups have been observed in propane, butane and pentane. Cyclic alkane feedstock, including cyclohexane and norbornane, could also be employed in this iron catalytic system to produce valuable carboxylic acid building blocks. This demonstrates that the Fe photocatalytic system presented herein could find wide applicability in a variety of alkane conversions.

In summary, we have developed a practical photocatalytic protocol for the aerobic oxidative carbonylation of methane. Under LED irradiation at ambient temperature, acetic acid can be produced at high levels of efficiency and selectivity by abundant and inexpensive iron photocatalysts. We anticipate that further operando spectroscopic studies will provide more mechanistic details and guide the development of more efficient catalysts. We envision that the exploitation of the photoinduced iron-LMCT system and radical-metal combination strategy will provide new avenues towards the development of diverse alkane conversions under practical conditions.

References

1 Gunsalus, N. J. *et al*. Homogeneous Functionalization of Methane. *Chem. Rev*. **117**, 8521-8573, (2017).

2 Meng, X. *et al*. Direct Methane Conversion under Mild Condition by Thermo-, Electro-, or Photocatalysis. *Chem* **5**, 2296-2325 (2019).

3 Lin, M. & Sen, A. Direct catalytic conversion of methane to acetic acid in an aqueous medium. *Nature* **368**, 613, (1994).

4 Zerella, M., Mukhopadhyay, S. & Bell, A. T. Direct oxidation of methane to acetic acid catalyzed by Pd2+ and Cu2+ in the presence of molecular oxygen. *Chem. Commun*., 1948-1949, (2004).

5 Zerella, M., Kahros, A. & Bell, A. Methane oxidation to acetic acid catalyzed by Pd2+ cations in the presence of oxygen. *Journal of Catalysis* **237**, 111-117, (2006).

6 Shan, J., Li, M., Allard, L. F., Lee, S. & Flytzani-Stephanopoulos, M. Mild oxidation of methane to methanol or acetic acid on supported isolated rhodium catalysts. *Nature* **551**, 605-608, (2017).

7 Tang, Y. *et al*. Single rhodium atoms anchored in micropores for efficient transformation of methane under mild conditions. *Nat. Commun*. **9**, 1231, (2018).

8 Moteki, T., Tominaga, N. & Ogura, M. CO‐Assisted Direct Methane Conversion into C1 and C2 Oxygenates over ZSM‐5 Supported Transition and Platinum Group Metal Catalysts Using Oxygen as an Oxidant. *ChemCatChem* **12**, 2957-2961, (2020).

9 Nacsa, E. D. & MacMillan, D. W. C. in *Organic Reactions* 471-546 (2019).

10 Twilton, J. *et al*. The merger of transition metal and photocatalysis. *Nat. Rev. Chem*. **1**, 0052, (2017).

11 Levin, M. D., Kim, S. & Toste, F. D. Photoredox Catalysis Unlocks Single-Electron Elementary Steps in Transition Metal Catalyzed Cross-Coupling. *ACS Cent. Sci*. **2**, 293-301, (2016).

12 Kalyani, D., McMurtrey, K. B., Neufeldt, S. R. & Sanford, M. S. Room-Temperature C–H Arylation: Merger of Pd-Catalyzed C–H Functionalization and Visible-Light Photocatalysis. *J. Am. Chem. Soc*. **133**, 18566-18569, (2011).

13 Ye, Y. & Sanford, M. S. Merging Visible-Light Photocatalysis and Transition-Metal Catalysis in the Copper-Catalyzed Trifluoromethylation of Boronic Acids with CF3I. *J. Am. Chem. Soc*. **134**, 9034-9037, (2012).

14 Creutz, S. E., Lotito, K. J., Fu, G. C. & Peters, J. C. Photoinduced Ullmann C-N Coupling: Demonstrating the Viability of a Radical Pathway. *Science* **338**, 647-651, (2012).

15 Tellis, J. C., Primer, D. N. & Molander, G. A. Single-electron transmetalation in organoboron cross-coupling by photoredox/nickel dual catalysis. *Science* **345**, 433-436, (2014).
16 Zuo, Z. *et al*. Merging photoredox with nickel catalysis: Coupling of α-carboxyl sp3-carbons with aryl halides. *Science* **345**, 437-440, (2014).
17 Torres, G. M., Liu, Y. & Arndtsen, B. A. A dual light-driven palladium catalyst: Breaking the barriers in carbonylation reactions. *Science* **368**, 318-323, (2020).
18 Paulik, F. E. & Roth, J. F. Novel catalysts for the low-pressure carbonylation of methanol to acetic acid. *Chem. Commun*., 1578a, (1968).
19 Forster, D. Mechanistic Pathways in the Catalytic Carbonylation of Methanol by Rhodium and Iridium Complexes. *Adv. Organomet. Chem* **17**, 255-267, (1979).
20 Liu, Q., Zhang, H. & Lei, A. Oxidative Carbonylation Reactions: Organometallic Compounds (R–M) or Hydrocarbons (R–H) as Nucleophiles. *Angew. Chem. Int. Ed.* **50**, 10788-10799, (2011).
21 Labinger, J. A. & Bercaw, J. E. Understanding and exploiting C–H bond activation. *Nature* **417**, 507-514, (2002).
22 Periana, R. A., Mironov, O., Taube, D., Bhalla, G. & Jones, C. Catalytic, Oxidative Condensation of CH4 to CH3COOH in One Step via CH Activation. *Science* **301**, 814-818, (2003).
23 Hu, A., Guo, J.-J., Pan, H. & Zuo, Z. Selective functionalization of methane, ethane, and higher alkanes by cerium photocatalysis. *Science* **361**, 668-672 (2018).
24 Laudadio, G. *et al*. C(sp3)–H functionalizations of light hydrocarbons using decatungstate photocatalysis in flow. *Science* **369**, 92-96, (2020).
25 Thomas, J. K. Pulse radiolysis of aqueous solutions of methyl iodide and methyl bromide. The reactions of iodine atoms and methyl radicals in water. *J. Phy. Chem.* **71**, 1919-1925, (1967).
26 Bakac, A., Espenson, J. H. & Young, V. G. Kinetics of acetyl radical formation from methyl radicals and carbon monoxide and crystal structures of two acetylcobalt complexes. *Inorg. Chem.* **31**, 4959-4964, (1992).
27 Chatgilialoglu, C., Crich, D., Komatsu, M. & Ryu, I. Chemistry of Acyl Radicals. *Chem. Rev.* **99**, 1991-2070, (1999).
28 Shu, L. *et al*. An Fe2IVO2 Diamond Core Structure for the Key Intermediate Q of Methane Monooxygenase. *Science* **275**, 515-518, (1997).
29 Huang, X. & Groves, J. T. Beyond ferryl-mediated hydroxylation: 40 years of the rebound mechanism and C–H activation. *J. Biol. Inorg. Chem.* **22**, 185-207, (2016).
30 Lin, M. & Sen, A. Oxidation and oxidative carbonylation of methane and ethane by hexaoxo-μ-peroxodisulfate(2–) ion in aqueous medium. A model for alkane oxidation through the hydrogen-atom abstraction pathway. *J. Chem. Soc. Chem. Comm*., 892-893, (1992).
31 Takahiro, N., Kazuyuki, N., Ken, T. & Yuzo, F. Transition Metal Catalyzed Acetic Acid Synthesis from Methane and CO. *Chem. Lett.* **21**, 1141-1142, (1992).
32 Asadullah, M., Kitamura, T. & Fujiwara, Y. Calcium-Catalyzed Selective and Quantitative Transformation of CH4 and CO into Acetic Acid. *Angew. Chem. Int. Ed.* **39**, 2475-2478, (2000).
33 Kirillova, M. V. *et al*. Direct and remarkably efficient conversion of methane into acetic acid catalyzed by amavadine and related vanadium complexes. A synthetic and a theoretical DFT mechanistic study. *J. Am. Chem. Soc.* **129**, 10531-10545, (2007).
34 Weiss, M. E., Kreis, L. M., Lauber, A. & Carreira, E. M. Cobalt-Catalyzed Coupling of Alkyl Iodides with Alkenes: Deprotonation of Hydridocobalt Enables Turnover. *Angew. Chem. Int. Ed.* **50**, 11125-11128, (2011).
35 Parasram, M., Chuentragool, P., Sarkar, D. & Gevorgyan, V. Photoinduced Formation of Hybrid Aryl Pd-Radical Species Capable of 1,5-HAT: Selective Catalytic Oxidation of Silyl Ethers into Silyl Enol Ethers. *J. Am. Chem. Soc.* **138**, 6340-6343, (2016).
36 Shields, B. J. & Doyle, A. G. Direct C(sp3)–H Cross Coupling Enabled by Catalytic Generation of Chlorine Radicals. *J. Am. Chem. Soc.* **138**, 12719-12722, (2016).
37 Ravetz, B. D., Wang, J. Y., Ruhl, K. E. & Rovis, T. Photoinduced Ligand-to-Metal Charge Transfer Enables Photocatalyst-Independent Light-Gated Activation of Co(II). *ACS Catal.* **9**, 200-204, (2018).
38 Bonin, J., Robert, M. & Routier, M. Selective and Efficient Photocatalytic CO2 Reduction to CO Using Visible Light and an Iron-Based Homogeneous Catalyst. *J. Am. Chem. Soc.* **136**, 16768-16771, (2014).
39 Rao, H., Schmidt, L. C., Bonin, J. & Robert, M. Visible-light-driven methane formation from CO2 with a molecular iron catalyst. *Nature* **548**, 74-77, (2017).
40 Bartocci, C. *et al*. Photoredox and photocatalytic characteristics of various iron meso-tetraarylporphyrins. *Inorg. Chem.* **30**, 1255-1259, (1991).
41 Maldotti, A. *et al*. Photochemistry of Iron-porphyrin complexes. Biomimetics and catalysis. *Coord. Chem. Rev.* **125**, 143-154, (1993).
42 Brault, D. & Neta, P. Reactions of iron porphyrins with methyl radicals. *J. Am. Chem. Soc.* **103**, 2705-2710, (1981).
43 Magnuson, R. H., Zulu, S., T'Sai, W.-M. & Giering, W. P. Detection and characterization of radical cations resulting from the oxidation of methyl and acetyl iron complexes. *J. Am. Chem. Soc.* **102**, 6887-6888, (1980).
44 Arafa, I. M., Shin, K. & Goff, H. M. Carbon monoxide and carbon dioxide carbon-metal bond insertion chemistry of alkyliron(III) porphyrin complexes. *J. Am. Chem. Soc.* **110**, 5228-5229, (1988).
45 An, Q. *et al*. Cerium-Catalyzed C–H Functionalizations of Alkanes Utilizing Alcohols as Hydrogen Atom Transfer Agents. *J. Am. Chem. Soc.* **142**, 6216-6226 (2020).

Acknowledgements: We thank the National Natural Science Foundation of China (21772121, 21971163) and Shell Global Solutions International B.V. for financial support.

Author contributions: Z.Z. conceived the research and designed the experiments with input of A.M., J.S. and A.P.B. H.P., Q.A. and H.C. prepared the catalysts and performed catalyst evaluation. Q.A. and Y.C. performed mechanistic investigations. All the authors participated in writing the manuscript.

Supplementary Materials

Materials and Methods
Supplementary Text
Figs. S1 to S11
Schemes S1 to S10
GC data and NMR spectra

Figures

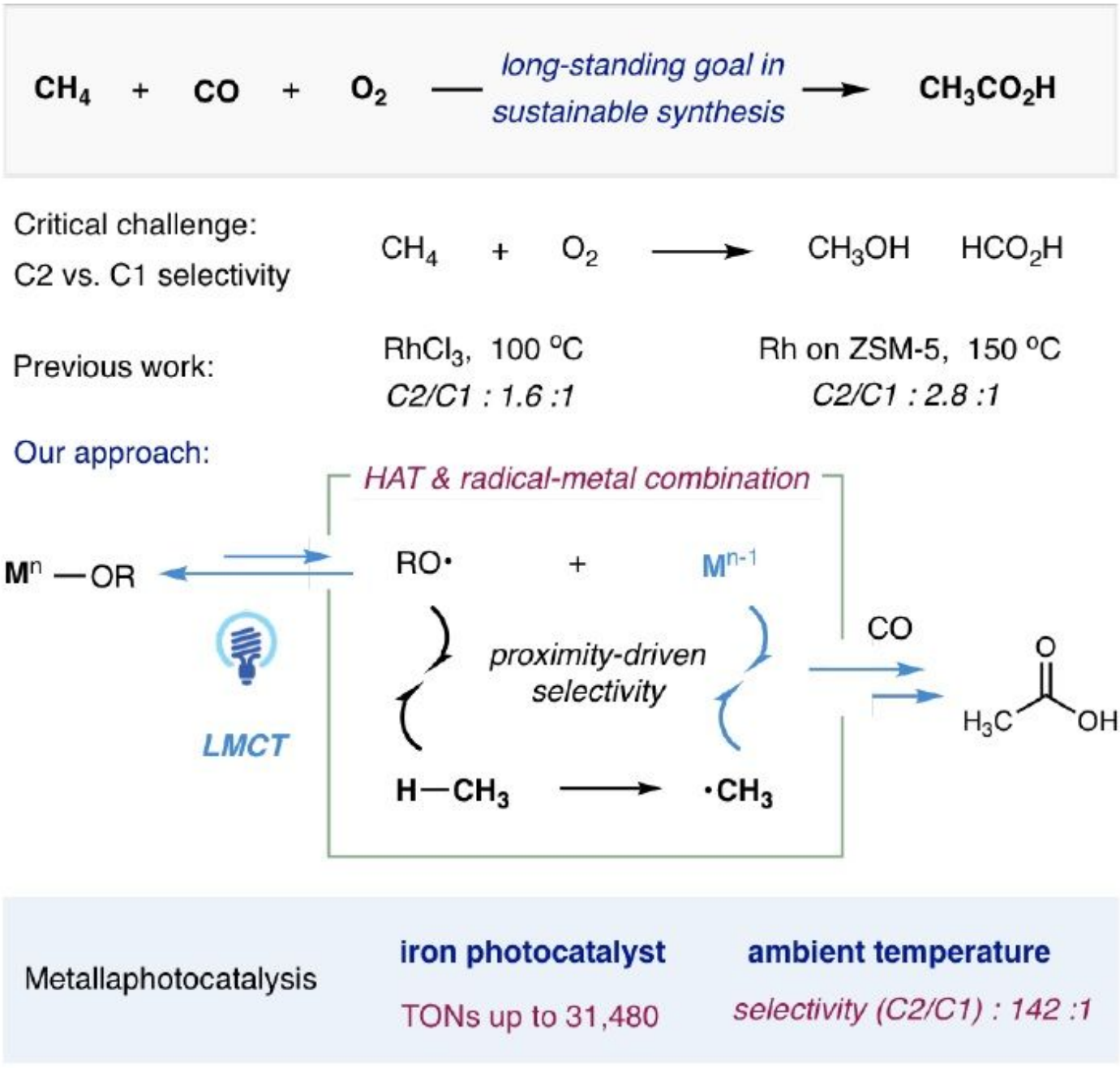

Figure 1

Photocatalytic aerobic oxidative carbonylation of methane by iron catalyst. A radical-metal combination merged with LMCT-homolysis was proposed to elude the nonselective methane oxidation for highly selective carbonylation.

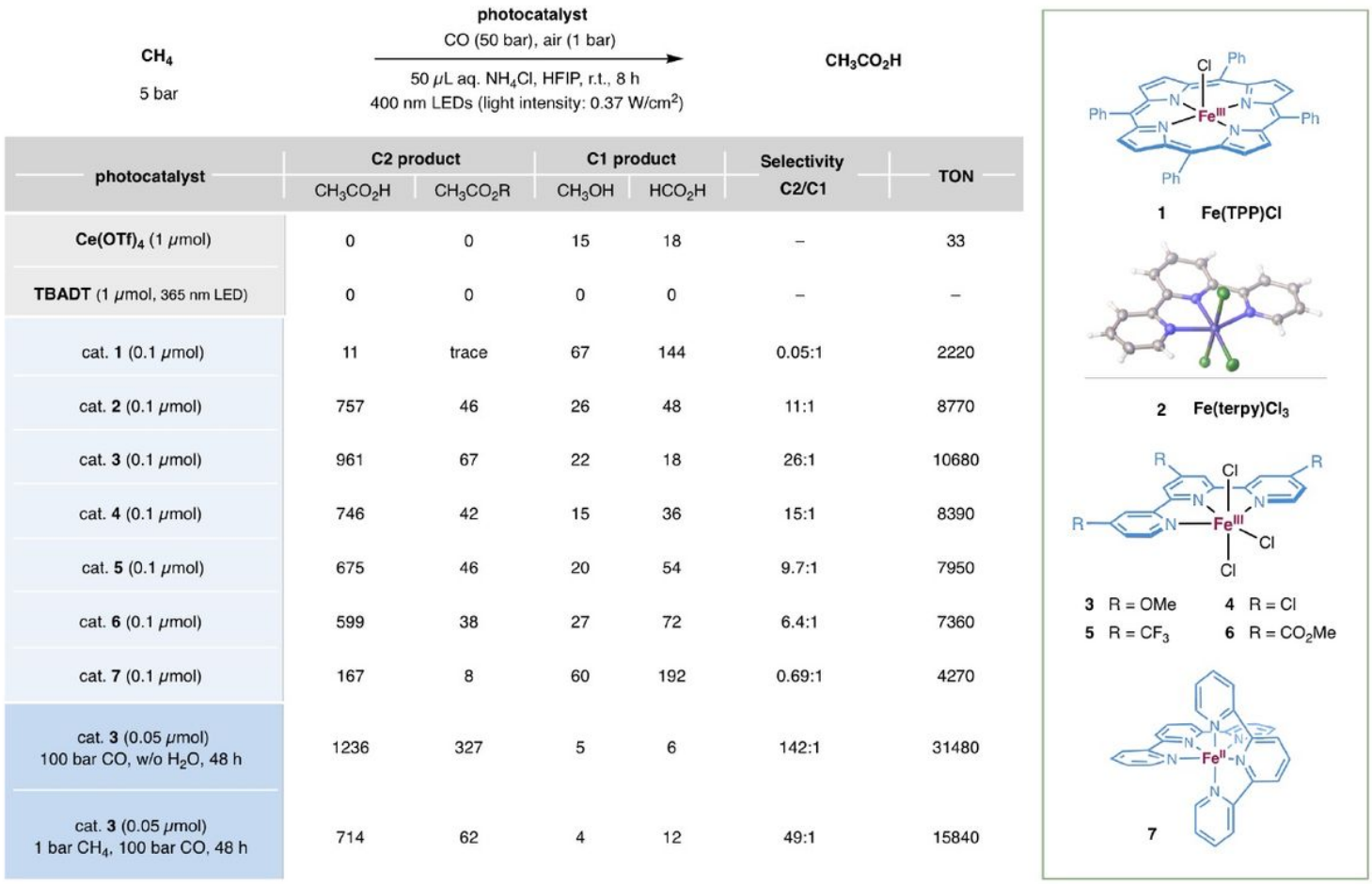

photocatalyst	C2 product		C1 product		Selectivity	TON
	CH_3CO_2H	CH_3CO_2R	CH_3OH	HCO_2H	C2/C1	
$Ce(OTf)_4$ (1 μmol)	0	0	15	18	–	33
TBADT (1 μmol, 365 nm LED)	0	0	0	0	–	–
cat. **1** (0.1 μmol)	11	trace	67	144	0.05:1	2220
cat. **2** (0.1 μmol)	757	46	26	48	11:1	8770
cat. **3** (0.1 μmol)	961	67	22	18	26:1	10680
cat. **4** (0.1 μmol)	746	42	15	36	15:1	8390
cat. **5** (0.1 μmol)	675	46	20	54	9.7:1	7950
cat. **6** (0.1 μmol)	599	38	27	72	6.4:1	7360
cat. **7** (0.1 μmol)	167	8	60	192	0.69:1	4270
cat. **3** (0.05 μmol) 100 bar CO, w/o H_2O, 48 h	1236	327	5	6	142:1	31480
cat. **3** (0.05 μmol) 1 bar CH_4, 100 bar CO, 48 h	714	62	4	12	49:1	15840

Figure 2

Selective aerobic oxidative carbonylation of methane. Yields and ratios of all products were determined by GC, 1H NMR analysis with internal standard. See full details in Supporting materials. R = OCH(CF3)2.

Image not available with this version

Figure 3

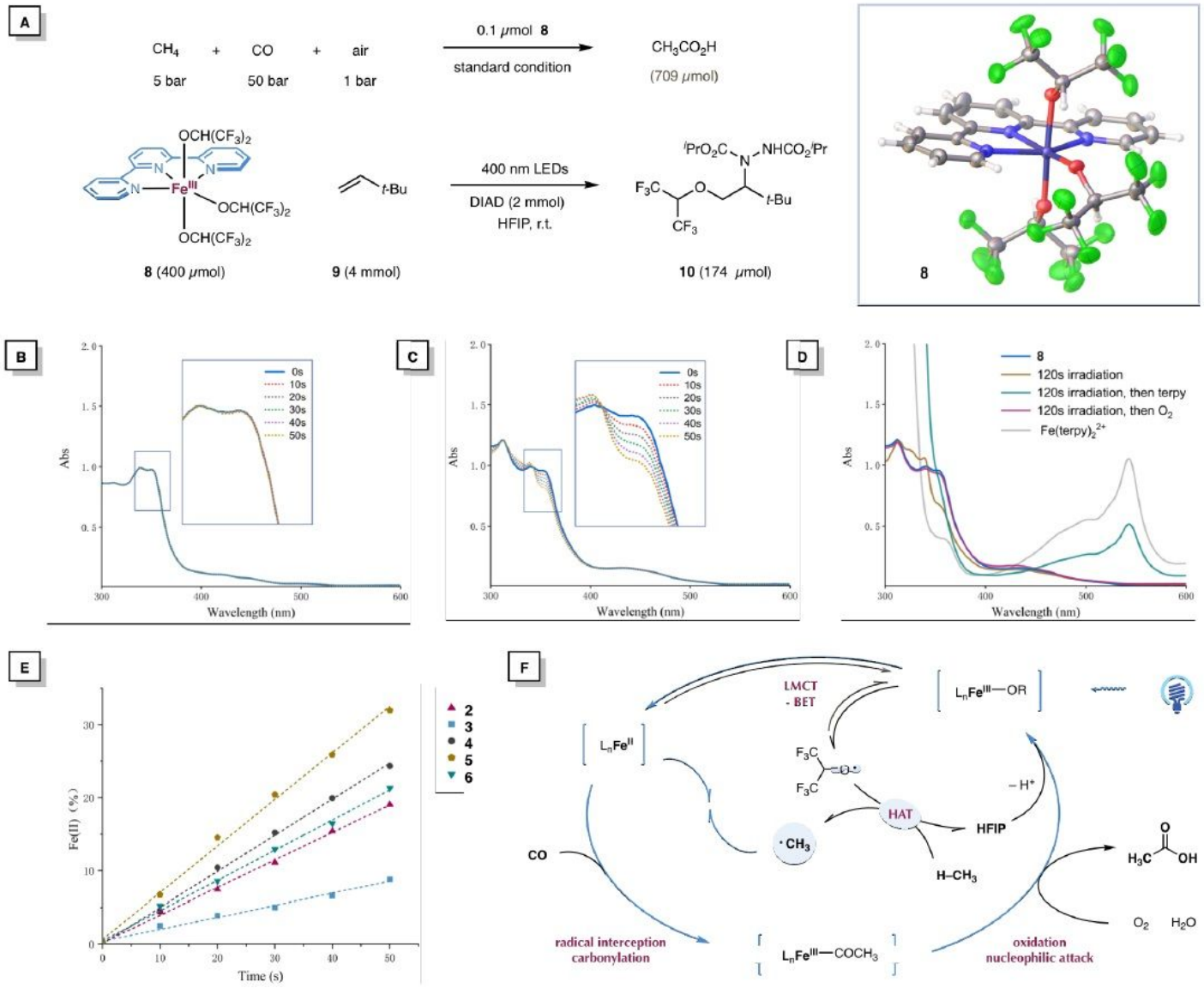

Figure 4

Mechanistic investigations. (A) Structure elucidation of complex 8 and radical-trapping experiment. (B) Photolysis of complex 8 in HFIP. (C), (D), Photolysis of complex 8 in HFIP, in the presence of neohexene (0.4 M). (E) photolysis rates of various iron alkoxide complexes in the presence of neohexene (0.4 M). (F) A proposed model for the photocatalytic aerobic carbonylation of methane. R = OCH(CF3)2.

Supplementary Files

This is a list of supplementary files associated with this preprint. Click to download.

- SI202012062.pdf
- scheme1.png
- scheme2.png